Optics and Lasers in Engineering 148 (2022) 106755

Contents lists available at ScienceDirect

Optics and Lasers in Engineering

journal homepage: www.elsevier.com/locate/optlaseng

A method to eliminate the matching problem and improve the spectral property of Talbot spectrometer

Yixuan Li[a,b], Yu Huang[a,*], Haochen Li[a,b], Xiaohu Yang[a], Zhanfeng Li[a], Zihui Zhang[a], Shurong Wang[a,c,*]

[a] Changchun Institute of Optics, Fine Mechanics and Physics, Chinese Academy of Sciences, Changchun, 130033, China
[b] University of Chinese Academy of Sciences, Beijing, 100049, China
[c] Foshan University, Foshan, 528225, China

ARTICLE INFO

Keywords:
Talbot spectrometer
Mask of detector
Cover the (phase-inverted) self-imaging
Eliminate the matching problem

ABSTRACT

At present, the mutual restriction between the spectral resolution and the dynamic range limits the further improvement of the spectral property of Talbot spectrometer. This mutual restriction is caused by the matching problem of grating and detector. Here, a method, which focuses on eliminating the relationship between grating and detector in the design of Talbot spectrometer, for masking detector to cover the (phase-inverted) self-imaging is introduced. Both theoretical simulation and experimental analysis validate the method, which maintains the contrast of pattern while changing the size of pixels and thus the matching problem no longer exists. Overall, this method breaking the bottleneck of spectral property for current talbot spectrometers, which makes the system design more flexible and enhances the universality of Talbot spectrometer, and the spectral resolution of the spectrometer under this method can be superior to 0.3nm while keeping the contrast of pattern, better than the previously reported best spectral resolution 1nm of current talbot spectrometer.

Introduction

A periodic pattern of "Talbot self-imaging" can be observable behind the grating immediately when a periodic structure such as a grating is illuminated with spatially coherent light [1]. This phenomenon is called "Talbot effect", which has been widely used for interferometer [2-4], integrated optics [5-7], nonlinear optics [8, 9], quantum optics [10-12], lithography [13,14], and calibrate microscopy [15]. Besides, Talbot effect has been previously proposed as the building component for realizing spectrometers because of its interferometric nature with an invertible spatio-spectral response [16-19]. It should be noted that the period of Talbot pattern is identical with the grating, and halfway between the self-imaging planes are the phase-inverted imaging planes, whose light and dark regions are contrary to self-imaging planes [19]. Thus, to obtain all information of the Talbot pattern, a sampling frequency that reached the Nyquist Sampling Theorem requested should be used, and a higher density of grating is also required to reach a higher spectral resolution. However, smaller pixel pitch means a smaller and more unstable imager, which limits the OPD (Optical Path Difference) and other properties. In addition, the smallest commercially available imager pixel size is on the order of a micron, which means the sampling frequency is much lower than the Nyquist Sampling Theorem requested. Therefore, the detector and grating need to be matched strictly. Current Talbot spectrometers have reached 1nm spectral resolution by strictly matching detector and grating, where are three lines imaged onto the same pixel of the imager [19, 20]. The further promotion of Talbot spectrometer required technological progress of detector or a method to eliminate the matching problem. There has been an effort to break through this limitation. For example, there have been reports of using signal processing to achieve a blinding spectrum resolution of 10pm [21]. However, this method just can be used as a wavemeter rather than a general-purpose spectrometer.

We investigate a method that to break through the limitation of spectral property of current Talbot spectrometer and to eliminate the influence of matching of sensor and grating in the spectral property. Two sinusoidal gratings with the same period have been used in this spectrometer, one is used to generate Talbot pattern and another one is used as a mask to cover the (phase-inverted) self-imaging. Ideally, all (phase-inverted) self-imaging would be covered by the second grating. This method makes Talbot spectrometer with both high-density gratings and large pixel imager possible, the potential application of the Talbot spectrometer has been enhanced greatly.

* Corresponding authors.
E-mail addresses: ssshycn@163.com (Y. Huang), srwang@ciomp.ac.cn (S. Wang).

https://doi.org/10.1016/j.optlaseng.2021.106755
Received 23 March 2021; Received in revised form 15 June 2021; Accepted 22 July 2021
Available online 31 July 2021

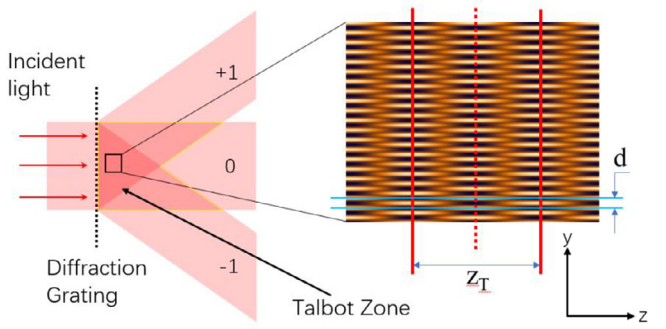

Fig. 1. Illustration of Talbot effect. There are only -1, 0, and +1 diffract orders after sinusoidal grating. The area inside the yellow lines on the left is Talbot zone. And on the right is Talbot pattern, where the solid red lines represent the self-imaging planes, the dotted line represents the phase-inverted self-imaging plane, the distance z_T between adjacent self-imaging planes can be calculated by equation (1), and the period d along the y-axis is the same as the period of the diffraction grating.

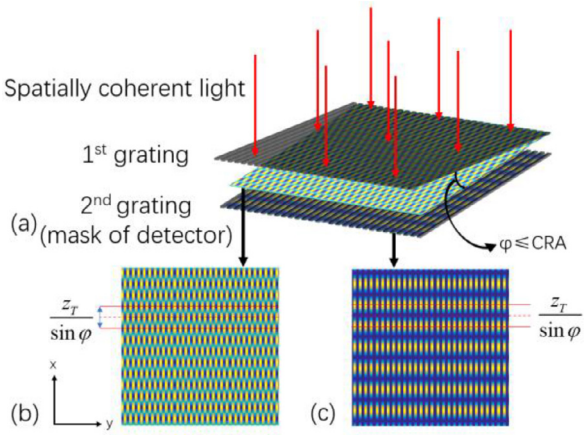

Fig. 2. (a) Illustration of Talbot spectrometer with detector mask. (b) The Talbot pattern before the mask of detector, where shows the self-imaging planes (solid red lines and spaced by $z_T/\sin\varphi$) and the phase-inverted self-imaging planes (dashed red line). (c) The Talbot pattern after the mask of detector.

Method

Talbot effect was first observed by H. F. Talbot in 1836 [1], and studied by Lord Rayleigh subsequently, who first gives the universal expression of the distance z_T between adjacent self-imaging planes [22]:

$$z_T = \frac{\lambda}{1-\sqrt{1-\frac{\lambda^2}{d^2}}} \tag{1}$$

Here λ is the wavelength, d is the grating period. The Talbot effect can only be observed up to a distance W / tan φ, behind the grating, where W is the width of the grating and the φ is the angle of the diffracted beam [16]. Since there is a one-to-one correspondence between the distance z_T and the wavelength λ, the Talbot pattern can be used to perform the spectral reconstruction. One requirement for the reconstruction of the spectrum of incident light: the difference between reversal and image planes can be recognized. Which can be seen in Fig. 1, where the solid red lines represent the self-imaging planes, the dotted line represents the phase-inverted self-imaging plane, the distance z_T between adjacent self-imaging planes can be calculated by equation (1). The smallest commercially available imager pixel size is on the order of a micron, which restricts the minimum period of the grating. This factor must not neglect in the design of Talbot spectrometer, or more than one line would be imaged onto the imager, which would reduce the ability of the system to resolve the Talbot effect.

When the self-imaging or inverse self-imaging has been covered by the second grating, which clings to the surface of the detector and the same as the first grating, only the inverse self-imaging or self-imaging can reach the surface of the detector. This means the difference between reversal and image planes can be recognized easily, and the limitation of pixel pitch is changed from the grating density to the sampling of interference fringe.

We expand on the basic design presented in [19]. A 1-D Sinusoidal amplitude transmission grating is normalized to incident spatially coherent light, and the grooves are aligned with the x-axis. Overlap another grating and an imager carefully so there are no gaps. It should be noted that despite this configuration have resemblances with moire deflectometry, they are different in principle. The second grating in our configuration is used as a mask of detector.

In Fig. 2, define x-direction of the detector as spectral dimension, and y-direction of the detector as periodical dimension. We tilt the detector with mask along the y-axis as shown in fig. 2, the maximum magnitude of inclination depends on the CRA (Chief Ray Angle) of imager. Those gratings have the same grating period d [Fig. 2(a)]. The incident light of this kind of spectrometer is spatially coherent light. Fig. 2(b) shows the Talbot pattern before the mask of detector, and Fig. 2(c) shows the Talbot pattern after the mask of detector. It is apparent that there is only self-imaging in the Talbot pattern after detector mask, which means the phase-inverted self-imaging planes of Talbot pattern have been covered after masking of detector. In this situation, the sampling along y-direction (periodical dimension) no longer affects the sampling along x-direction (spectral dimension).

It should be noted that the zero-path length would be the first grating and imager touching. Since this cannot be zero, there is a limit on the optical bandwidth that can be practically measured. For Talbot spectrometer, we should integrate the grating and imager to address this limitation. This paper lays stress on the factors of the limit of spectral property in current Talbot spectrometer and proposes a solution to improve the spectral resolution. Therefore, we use a laser interferometer (ZYGO Verifire^{TM}) as the source.

For the specific wavelength λ, the number of planes can be calculated by the following equation:

$$N = k \cdot D = \frac{D\sin\varphi}{z_T} = \frac{D(1-\sqrt{1-\frac{\lambda^2}{d^2}})\sin\varphi}{\lambda} \tag{2}$$

where k is the spaced frequency along the spectral dimension of imager, D is the length of the spectral dimension of imager, φ is the tilt of the imager. Two nearby wavelengths can be distinguished if ΔN=1. In this regime the resolution criterion implies that

$$\Delta\lambda = |\lambda_1 - \lambda_2| = \frac{2d^2 D\sin\varphi}{d^2 + D^2\sin^2\varphi} \tag{3}$$

Similarly, the resolution in the condition of paraxial can be implied as:

$$\Delta\lambda = |\lambda_1 - \lambda_2| = \frac{2d^2}{D\sin\varphi} \tag{4}$$

which is similar to [16] (magnification=1). The constraining factors for spectral resolution of the Talbot spectrometer are 1) the period of the grating, 2) the spectral dimension length of the imager, 3) the angle of rotation of the imager. Enhancing spectral resolution is equal to increasing the number of planes seen by the imager. The spectral dimension length of the imager depends on the pixel pitch and the number of pixels. The smallest commercially available imager pixel size is on the order of a micron, which restricts the smallest period of the optional gratings. For imager in current Talbot spectrometer, the requirements of pixel pitch are different between spectral dimension and period dimension: 1) the spectral dimension requires the pixel pitch in a range rather than limits to a definite value; 2) the period dimension needs smaller

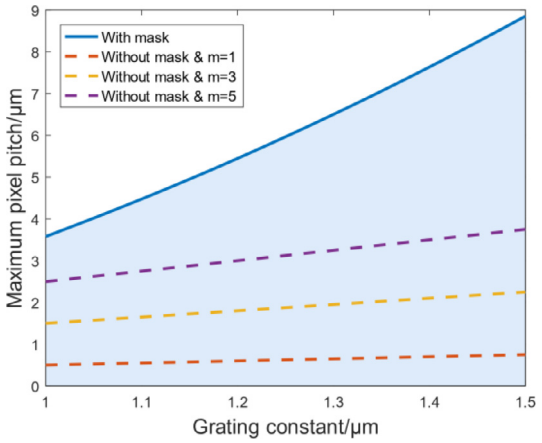

Fig. 3. This figure is drawn based on φ=20° and λ<0.7μm. The blue area is shown the range, along the Spectrum dimension of detector, of pixel pitch under different grating constant with detector mask. The dotted lines are shown the value of pixel pitch under different grating constant without detector mask. For Talbot spectrometer with detector mask, when the pixel pitch of detector falls in the blue area, the oscillation along the Spectrum dimension can be received. For current Talbot spectrometer, when "m" and grating constant are determined to be a certain value, pixel pitch is a definite value. Here "m" is the ratio of the pixel pitch of detector and the half of grating period.

pixel pitch than spectral dimension [Fig. 3]. The blue area in Fig. 3 is calculated by the following equation:

$$P \le \frac{1}{2k} = \frac{\frac{1}{2}\cdot\lambda}{(1-\sqrt{1-\frac{\lambda^2}{d^2}})\sin\varphi} \tag{5}$$

Where P is the range of pixel pitch with detector mask, k is the spaced frequency along the spectral dimension of imager, d is the grating constant, φ is the tilt of the imager. And the dotted lines in Fig. 3 can be calculated by the following equation:

$$P_m = m\cdot\frac{d}{2} \qquad (m = 1, 3, 5, 7...) \tag{6}$$

For the Talbot spectrometer without detector mask, the pixel pitch must satisfy the sampling in both dimensions of detector. For the Talbot spectrometer proposed in this paper, by contrast, the pixel pitch only needs to satisfy the Nyquist sampling in spectral dimension. This means the design of Talbot spectrometer with both high-density gratings and large pixel imager is possible, and the resolution of imager is finite, hence, the length of the imager is proportional to the pixel pitch under the same resolution of imager. It can be seen from equation (4) that the bigger detector size is, or the smaller grating constant is, the higher spectral resolution is, thereby enhancing the spectral resolution of Talbot spectrometer while maintaining the high dynamic range.

To outstanding the advantage of Talbot spectrometer with detector mask compared to current Talbot spectrometer, we need to ensure that all factors are all the same apart from the mask of detector. We used two transmission grating (Tripolar Optoelectronics 300lines/mm) with a grating period of d=3.33 microns and a monochrome CMOS imager (Aptina MT9J003) with pixel pitch p=1.67 microns, and 3840 × 2748 pixels (active imager size 6.413 mm (H) × 4.589 mm (V)) in size. The first grating is used to generated Talbot pattern, and the second grating, which plane of grooves of the grating is glued to the imager [Fig. 4(a)], is used as a mask of detector. To receive an accurate angle between the first grating and imager, the camera has been fixed on a turntable [Fig. 4(b)]. The optical setup is shown in Fig. 4(c). When the second grating is removed the Talbot spectrometer with detector mask had changed to the current Talbot spectrometer. The camera rotated at an angle of φ=13.4° (CRA of MT9J003 is 13.4°) was used to generate the Talbot self-images. Talbot patterns of both cases can be received, respectively.

Results and discussions

For the method presented in this paper, the key to enhancing spectral resolution is to eliminate the matching problem between the grating and the detector, making the design of Talbot spectrometer with both high-density gratings and large pixel imager is possible. To verify our method, we contrast spectrometers in two different setups, one is a setup with detector mask and another one is a setup without detector mask and observed their performance at various pixel pitch. The pixel pitch of imager is changed by binning, in this case, the equivalent pixel pitch be 1.67 microns [Fig. 5 (a), Fig. 6 (a)], 3.33 microns [Fig. 5 (b), Fig. 6 (b)], 5 microns [Fig. 5 (c), Fig. 6 (c)] and 6.67 microns [Fig. 5 (d), Fig. 6 (d)]. Fig. 5 and Fig. 6 show the theoretical signal, original signal and frequency domain (reconstructed spectrum) generated under setup without detector mask and setup with detector mask, respectively. All theoretical images and original images are shown a 641μm × 460μm subsection of the entire image.

Since there are machining errors of both imagers and gratings, the Talbot pattern received of imager is modulated by moire fringe [Fig. 5 (a2~d2), Fig. 6 (a2~d2)]. As shown in the raw images, there is an oscillation in the intensity across the row of the CMOS imager. This oscillation period is proportional to that of the Talbot period and can be used to reconstruct the spectrum of the incident light. It can be seen from Fig. 5 (a3~d3) that the dynamic range of the spectrum decreases along with the decrease of contrast of the raw image. The dynamic range of the reconstructed spectrums in Fig. 6 (a3~d3), by contrast, are similar to each other.

The OPDs are same in the different cases. As mentioned before, "m" is the ratio of the pixel pitch of detector and the half of grating period. Current Talbot spectrometers with different "m" are quite different in the signals. Specifically, effective information in Talbot pattern would be covered by noise when "m" is an even number, the manifestations of this case are a blur in original images, falling contrast of Talbot pattern, and spectral resolution decline; on the other hand, though the effective information of incident light could be extracted from raw signals directly when "m" is an odd number, the spectral resolution and contrast of Talbot patterns are both declined as "m" increasing. It should be noted that for self-imaging (or phase-inverted self-imaging), the phase-inverted self-imaging (or self-imaging) would be deemed to the main noise in the process of Talbot signal acquisition. In contrast, for the setup with detector mask proposed in this paper, there seems to be little difference of signals whether the "m" is an odd number or even number [Fig. 7]. This means Talbot spectrometer with both high-density grating and large pixel detector possible. In addition, there have fewer slight peaks as "m" equal to 1, while the intensity of those peaks tends to damp or vanish when "m" is larger than 1, which means the detector with large pixel pitch used in the Talbot spectrometers not only maintains the good contrast but also reduce the noise. The interference fringe contrast in Fig. 7 is calculated by the following equation:

$$V = \frac{1}{n}\cdot\sum_{i=1}^{n}\frac{I_{iM}-I_{im}}{I_{iM}+I_{im}} \tag{7}$$

Where V is the interference fringe contrast, n is the number of lines along the periodical dimension, I_{iM} is the average value of all the peaks in the interference fringe on row i, I_{im} is the average value of all the valleys in the interference fringe on row i.

Our experimental results are largely consistent with our theoretical model. However, there are a few issues with the results.

The first is the original images of the setup with detector mask, which are different from the theoretical images. This can be explained by the machining error of gratings and detectors.

Second, we had used a grating as a mask of detector. Although a grating has been added, which do not increase complexity of aligning because the aligning of grating and detector is equivalent to the aligning of grating and mask.

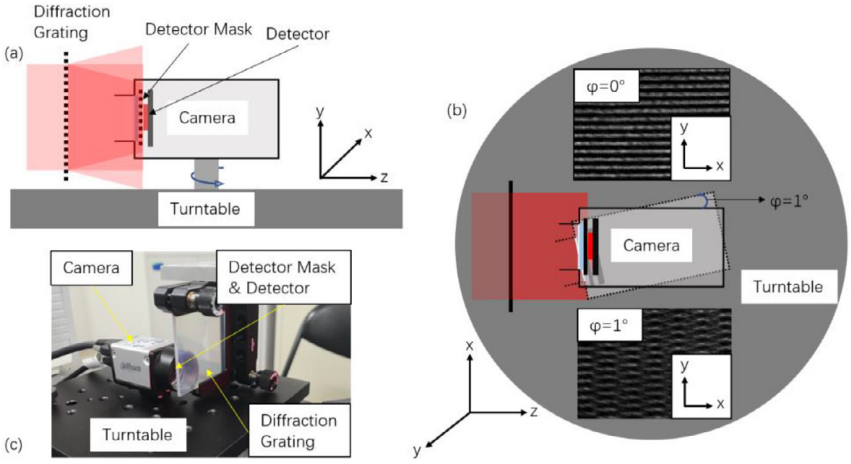

Fig. 4. (a) Illustration showing the instruction of the experimental setup. The self-images are formed in the mid-field where the ±1 and 0 diffracted beams interfere. The detector mask, which was fixed between the optical windows and the imager, is used to cover the self-images or inverse self-images. (b) Overhand view of the experimental setup. On the two insets (φ=0° and φ=1°), the intensity distribution along the Y-axis is independent of the imager tilt, which proved that there is a machining error between the grating and the mask of detector. (c) Photograph of the experimental setup. The camera is mounted on the turntable, and the diffraction grating is inverted mounting on a fixed mount, which is not touched the turntable.

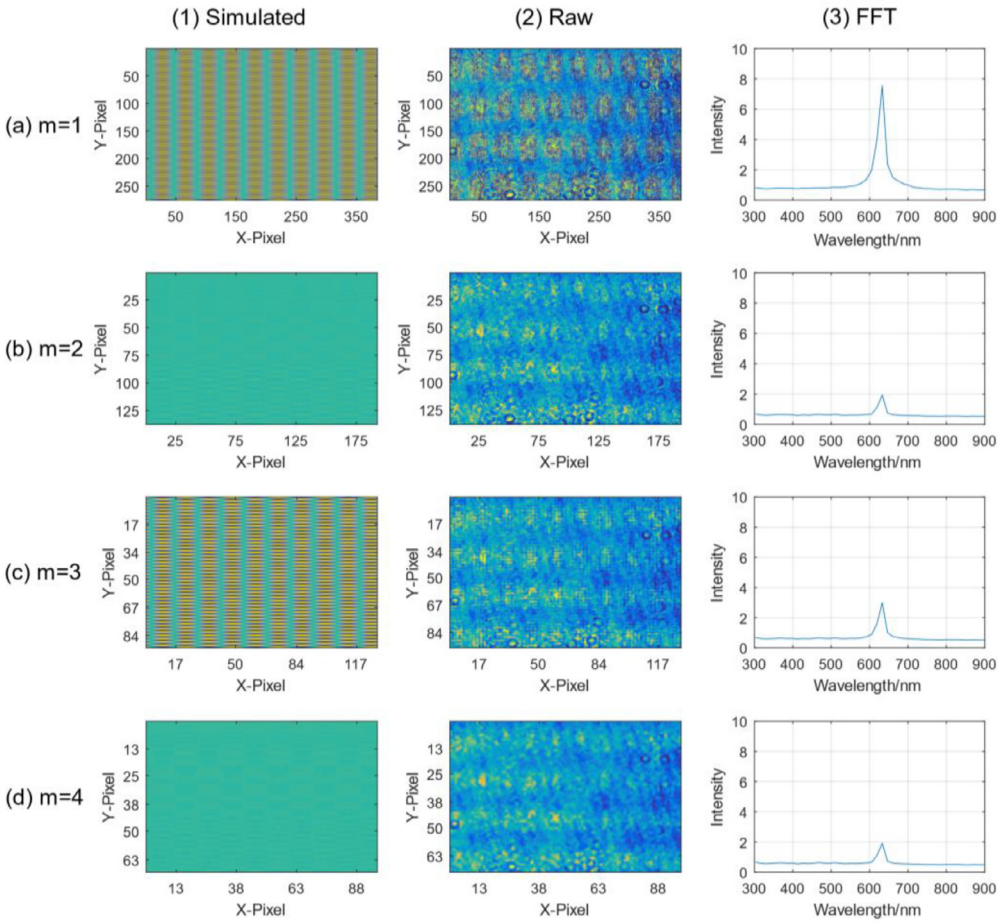

Fig. 5. Part of the simulated image, raw image, and frequency domain curve (corresponding spectrum with an equivalent pixel pitch of (a)1.67 microns, (b)3.33 microns, (c)5 microns, and (d)6.67 microns) generated under setup without detector mask. The contrasts of raw images are (a2) 50.79%, (b2) 2.71%, (c2) 24.25%, and (d2) 2.41%. The operating wavelength was 632.8nm. The FWHM of the peak in reconstructing spectrums are (a3) 25.21nm, (b3) 30.17nm, (c3) 26.18nm, and (d3) 29.18nm. In the images, the x-axis and y-axis are along the spectral dimension and the periodical dimension, respectively.

Third, the contrast of Talbot pattern in Fig. 5 (a2) is below the image received under setup with detector mask in Fig. 6 (a2). This, in part, is due to the accuracy of grating is greatly better than the accuracy of the pixel pitch of detector, but also because of the crosstalk between neighboring pixels. For the setup with detector mask, there is no crosstalk to the pixels in dark areas since the dark areas are covered by the mask.

Fourth, the FWHM of the FT peak under the setup without detector mask is far worse than the theoretical resolution. This is both due to the lower accuracy of pixel pitch of detector and the crosstalk between neighbor pixels. As shown in the processed image of Fig. 8, which is the raw image in Fig. 5 (a2) after downsampling and stretching, there is a tiny spot between neighboring hot spots. Which also proved that a setup with detector mask is more robust than a setup without detector mask. It should be noticed that the multiple of downsampling and stretching is 2.

Lastly, the FWHM of the FT peak in the setup with detector mask is about 14.4 nm, slightly greater than the best resolution of 14.92nm calculated by equation (4). This could be due to inaccuracy of the grating density, size of the image sensor, and rotate angle, which makes a tiny error in theoretical spectral resolution.

The experiment shows that the influence of pixels size in the process of reconstructing spectrum can be declined in our setup with detector mask. For the setup without detector mask, the “m” is an accurate odd number, which is an essential precondition for the detector to receive

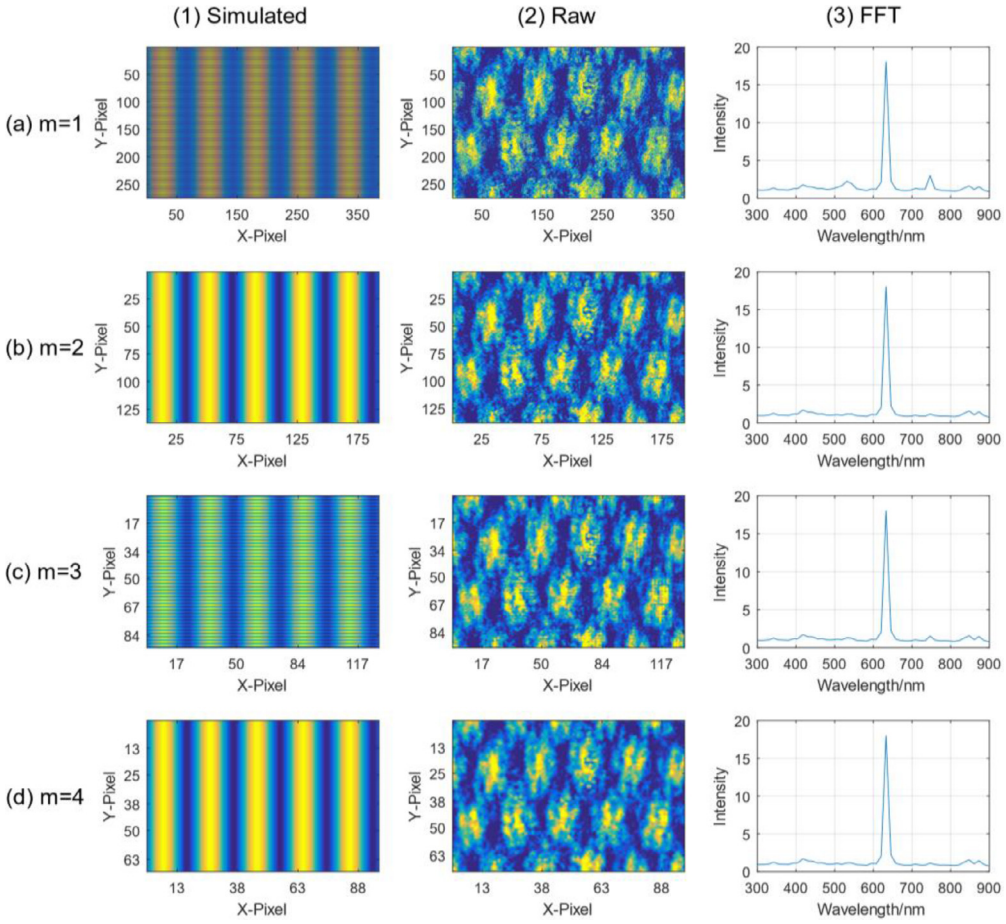

Fig. 6. Part of the simulated image, raw image and frequency domain curve (corresponding spectrum with an equivalent pixel pitch of (a)1.67 microns, (b)3.33 microns, (c)5 microns, and (d)6.67 microns) generated under the setup with detector mask. The contrasts of raw images are (a2) 57.78%, (b2) 62.40%, (c2) 58.54%, and (d2) 53.06%. The operating wavelength was 632.8nm. The FWHM of the peak in reconstructing spectrums are (a3) 14.41nm, (b3) 14.37nm, (c3) 14.36nm, and (d3) 14.35nm. In the images, the x-axis and y-axis are along the spectral dimension and the periodical dimension, respectively.

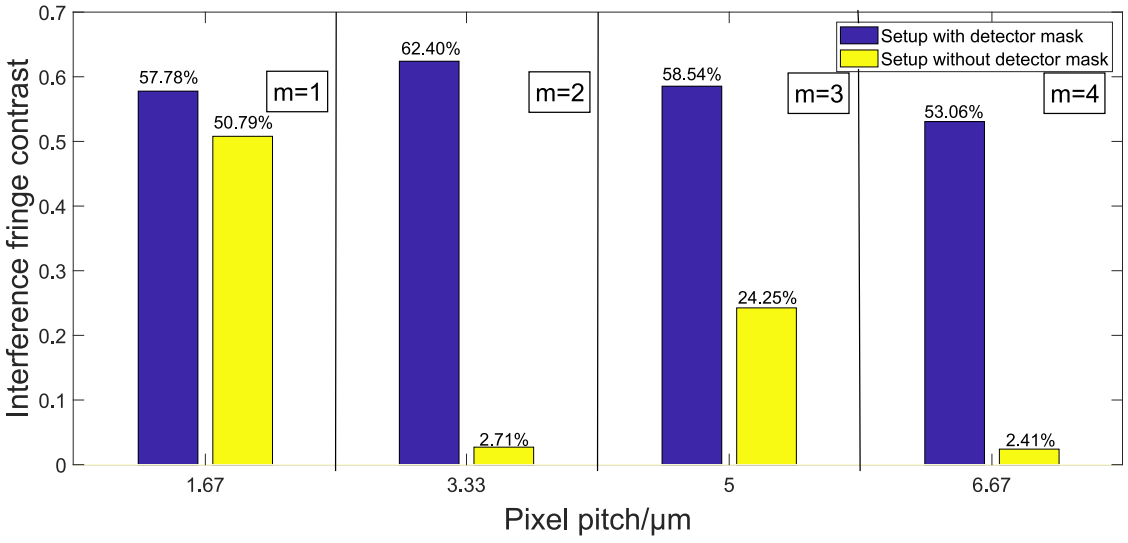

Fig. 7. The contrasts of the raw images generated under the setup with detector mask are 57.78% (m=1, d=3.33μm), 62.40% (m=2, d=3.33μm), 58.54% (m=3, d=3.33μm), and 53.06% (m=4, d=3.33μm). For comparison, the contrasts of the raw images generated under setup without detector mask are 50.79% (m=1), 2.71% (m=2), 24.25% (m=3), and 2.41% (m=4).

a clear Talbot pattern. Especially, to get a better spectral resolution, "m" always bigger than 1, which results in a decrease in the contrast of the interference fringe. For the setup with detector mask, in contrast, the pixel pitch of detector just needs to be satisfied with the limitation from the range of under test spectrum. The method provided in this paper makes Talbot spectrometer with both high-density gratings and large pixel imager possible, which means the spectral resolution and the dynamic range of spectrum reconstructed from Talbot spectrometer improvements have been enormous. When the grating constant and rotate angle of camera are 1.035μm and 20° respectively, the theoretical

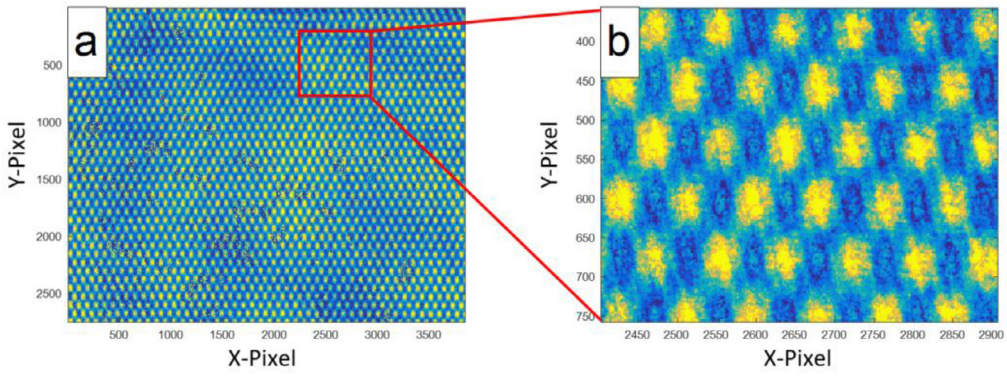

Fig. 8. (a) is the processed image (downsampling and stretching) of the setup without detector mask. (b) is a part of the processed image. In the images, the x-axis and y-axis are along the spectral dimension and the periodical dimension, respectively.

Table 1
Comparison of the Proposed Spectrometer and the latest previous Talbot spectrometer

Name	Dimensions	Wavelength Range	Resolution (FWHM)
Talbot with detector mask (CRA=20°)	<25mm × 25mm × 10mm	350nm~700nm	<0.3nm
Talbot without detector mask (CRA=20°)	10mm × 10mm × 6mm	520nm~1000nm	~1nm

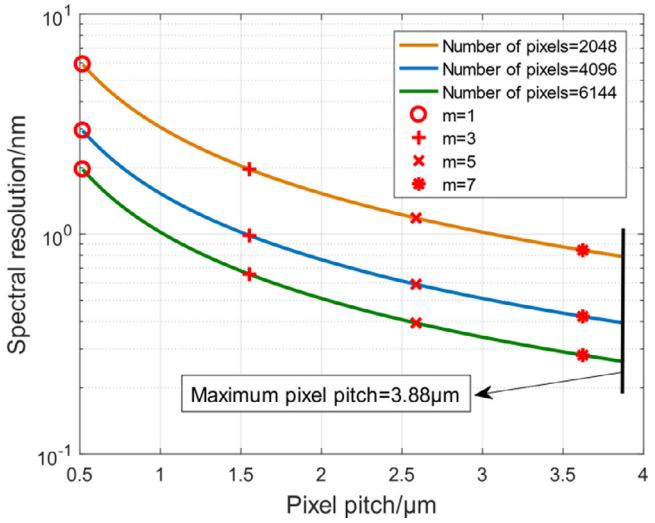

Fig. 9. This figure shows that in the case of the spectral range is 350nm~700nm and the grating constant and rotate angle of camera are 1.035μm and 20° respectively, the theoretical spectral resolution of Talbot spectrometer with different pixel pitch and number. The black line shows the maximum pixel pitch, in this case, is 3.88μm, which is calculated by equation (5). The numbers of pixels along spectral dimension of detector, from top to bottom, are 2048 (orange curve), 4096 (blue curve), and 6144 (green curve), respectively.

spectral resolution of Talbot spectrometer with different pixel pitches and pixel numbers are shown in Fig. 9. It should be noted that the solid lines show the case with detector mask, and the marks on the line show the case without detector mask. The spectral resolution of Talbot spectrometer with detector mask can be superior to 0.3nm in the spectral range of 350nm~700nm while maintaining the high contrast of pattern. To reach the same spectral resolution, the "m" should be 7 for Talbot spectrometer without detector mask, the theoretical interference fringe contrast is 9.09% in this situation and it means low dynamic range of the FFT. A comparison of the latest previous reported Talbot spectrometer [19], and the proposed spectrometer in this paper is presented in Table 1.

Conclusion

Our data demonstrate a design with detector mask of Talbot spectrometer which could reconstruct spectrum unimpeded by the matching of detector and grating. It makes Talbot spectrometer breaking the bottleneck of the spectral property. Contrast with the current Talbot spectrometer, the Talbot spectrometer with detector mask could achieve a higher spectral resolution while maintaining the big dynamic range. Towards comparison with current methods under the same condition, here we used low-density gratings and a small image sensor, which cause a low spectral resolution. In theory, the spectral resolution can be superior to 0.3nm in the spectral range of 350nm~700nm while maintaining the contrast of pattern. We expect that the spectrometer proposed in this paper can be used for some situations where is a high requirement for dynamic range, compact and spectral resolution. To achieve the full potential of the proposed Talbot spectrometer with detector mask, then there are plans to build a spectrometer with high-density grating and large imager, and integrating the mask into an image sensor.

Funding

National Natural Science Foundation of China (Nos. 41527806)

Declaration of Competing Interest

The authors declare that they have no known competing financial interests or personal relationships that could have appeared to influence the work reported in this paper.

CRediT authorship contribution statement

Yixuan Li: Conceptualization, Methodology, Investigation, Writing – original draft, Writing – review & editing. **Yu Huang:** Supervision, Project administration. **Haochen Li:** Software, Formal analysis. **Xiaohu Yang:** Resources, Formal analysis. **Zhanfeng Li:** Data curation. **Zihui Zhang:** Resources. **Shurong Wang:** Project administration, Funding acquisition.

References

[1] Talbot Henry Fox. LXXVI. Facts relating to optical science. No. IV. The London, Edinburgh, and Dublin Philosophical Magazine and Journal of Science 1836;9.56:401–7.

[2] Lohmann Adolf W, Silva DE. An interferometer based on the Talbot effect. Optics Communications 1971;2.9:413–15.
[3] Idrisov RF, et al. Inscription of superimposed fiber Bragg gratings using a Talbot interferometer. Journal of Optical Technology 2017;84.10:694–7.
[4] Dubey Rajiv, Kumar Raj. Comparison of sensitivity to beam collimation of the holographic shearing interferometer with the wedge plate shearing interferometer and the Talbot shearing interferometer. JOSA A 2020;37.9:B36–45.
[5] Iwanow Robert, et al. Discrete Talbot effect in waveguide arrays. Phys Rev Lett 2005;95.5:053902.
[6] Wang Yueke, et al. Discrete plasmonic Talbot effect in subwavelength metal waveguide arrays. Opt Lett 2010;35.5:685–7.
[7] Li Kai, et al. Discrete Talbot effect in dielectric graphene plasmonic waveguide arrays. Carbon 2017;118:192–9.
[8] Zhang Yong, et al. Nonlinear talbot effect. Phys Rev Lett 2010;104.18:183901.
[9] Deng Zhigui, et al. Talbot effect in waveforms containing subwavelength multilobe superoscillations. Opt Lett 2020;45.9:2538–41.
[10] Wen Feng, et al. Two-dimensional Talbot self-imaging via electromagnetically induced lattice. Sci Rep 2017;7.1:1–9.
[11] Farias Osvaldo Jimenez, et al. Quantum information processing by weaving quantum Talbot carpets. Phys Rev A 2015;91.6:062328.
[12] Sawada K, Walborn SP. Experimental quantum information processing with the Talbot effect. J Opt 2018;20.7:075201.
[13] Isoyan A, et al. Talbot lithography: Self-imaging of complex structures. Journal of Vacuum Science & Technology B: Microelectronics and Nanometer Structures Processing, Measurement, and Phenomena 2009;27.6:2931–7.
[14] Dunbar LA, et al. Talbot lithography as an alternative for contact lithography for submicron features. Advanced Fabrication Technologies for Micro/Nano Optics and Photonics VII, 8974. International Society for Optics and Photonics; 2014.
[15] Buitrago-Duque Carlos, Garcia-Sucerquia Jorge. Sizing calibration in digital lensless holographic microscopy via iterative Talbot self-imaging. Opt Lasers Eng 2020;134:106176.
[16] Kung Helen L, Bhatnagar Aparna, Miller David AB. Transform spectrometer based on measuring the periodicity of Talbot self-images. Opt Lett 2001;26.21:1645–7.
[17] De Nicola Sergio, et al. Talbot self-image effect in digital holography and its application to spectrometry. Opt Lett 2004;29.1:104–6.
[18] Sutham Witoon, et al. A novel spectrometer based on the near-field Talbot effect. J Phys Conf Ser 2017;901(1) IOP Publishing.
[19] Ye Erika, et al. Miniature, sub-nanometer resolution Talbot spectrometer. Opt Lett 2016;41.11:2434–7.
[20] Han Ningren, et al. Non-paraxial Talbot Effect for Building Compact Spectrometers." Computational Optical Sensing and Imaging. Optical Society of America 2016.
[21] Han Ningren, et al. Compact and high-precision wavemeters using the Talbot effect and signal processing. Opt Lett 2019;44.17:4187–90.
[22] Rayleigh Lord. XXV. On copying diffraction-gratings, and on some phenomena connected therewith. The London, Edinburgh, and Dublin Philosophical Magazine and Journal of Science 1881;11.67:196–205.